Catalysts **2015**, *5*, 518-533; doi:10.3390/catal5020518

OPEN ACCESS

catalysts

ISSN 2073-4344

www.mdpi.com/journal/catalysts

Article

Real-Time Raman Monitoring during Photocatalytic Epoxidation of Cyclohexene over V-Ti/MCM-41 Catalysts

Hsiang-Yu Chan [1], Van-Huy Nguyen [1,2], Jeffrey C.S. Wu [1,*], Vanesa Calvino-Casilda [3,†], Miguel A. Bañares [3] and Hsunling Bai [4]

[1] Department of Chemical Engineering, National Taiwan University, Taipei 10617, Taiwan; E-Mails: r99524020@ntu.edu.tw (H.-Y.C.); d10106811@mail.ntust.edu.tw (V.-H.N.)

[2] Department of Chemical Engineering, National Taiwan University of Science and Technology, Taipei 106, Taiwan

[3] Catalytic Spectroscopy Laboratory, Instituto de Catalisis, ICP-CSIC, E-28049 Madrid, Spain; E-Mails: vcalvino@ccia.uned.es (V.C.-C.); banares@icp.csic.es (M.A.B.)

[4] Institute of Environmental Engineering, National Chiao Tung University, Hsinchu 30010, Taiwan; E-Mail: hlbai@mail.nctu.edu.tw

† Current Address: Departamento de Quimica Inorganica y Quimica Tecnica, UNED, 28040 Madrid, Spain.

* Author to whom correspondence should be addressed; E-Mail: cswu@ntu.edu.tw; Tel.: +886-2-23631994, Fax: +886-2-23623040.

Academic Editor: Keith Hohn

Received: 28 November 2014 / Accepted: 17 March 2015 / Published: 30 March 2015

Abstract: A series of V- and/or Ti-loading MCM-41 catalysts are successfully synthesized with a hydrothermal method. The photocatalytic and thermal epoxidations of cyclohexene in the presence of *tert*-butyl hydroperoxide (*t*-BuOOH) were investigated with real-time monitored by NIR-Raman spectroscopy. It suggests that both V- and Ti-loading can be responsible for the cyclohexene epoxidation. Moreover, the complementary behavior of V- and Ti-loading may be related to a similar role of activation. Interestingly, the progress of the photo-epoxidation on $V_{0.25}Ti_2$/MCM-41 photocatalyst was monitored by changes in intensity of the characteristic Raman bands without interference from the UV-light irradiation. The result, for the first time, reveals that cyclohexene was directly photo-epoxidized to 1,2-epoxycyclohexane by *t*-BuOOH during the reaction. A possible mechanism of cyclohexene photo-epoxidation is also proposed for this study.

Keywords: cyclohexene; epoxidation; photocatalysis; V-Ti/MCM-41 photocatalyst; real-time Raman spectroscopy

1. Introduction

Nowadays, major epoxide chemicals, which are produced by epoxidation of olefins such as ethylene, propylene and cyclohexene, *etc.*, have become considerably more important, valuable and versatile intermediates in industrial organic synthesis [1–6]. Among epoxides, 1,2-epoxycyclohexane is an attractive chemical intermediates with multiple applications although it has been produced on the small scale only. For example, alicyclic molecule, which is synthesized from 1,2-epoxycyclohexane, is used in the production of pesticides, plant-protection agents, pharmaceuticals, perfumery, and dyestuffs. 1,2-epoxycyclohexane is also used as a monomer in polymerization with CO_2 to yield aliphatic polycarbonates [7]. Alternatively, it might be used for synthesis of chiral 1,2-amino alcohols and 1,2-diamines, which are known as the useful precursors of various chiral oxazolidinones, oxazinones, and phosphonamides, among others [8].

In cyclohexene epoxidation, to develop acceptable oxidative methodologies plays a major role from economic and environmental viewpoints. Among the oxidant agents for cyclohexene epoxidation, *tert*-butyl hydroperoxide (*t*-BuOOH) is the most popular. It has been extensively used due to its many advantages, such as its stability, mild oxidation, non-corrosive and non-hazardous properties. In addition, the separation process of by-products when using *t*-BuOOH is much easier than with others [9]. Another approach, which is based on utilizing clean and abundant photo-energy, instead of thermal energy, has been gained considerable interest. This concept, which directly produces 1,2-epoxycyclohexane under light radiation, is expected to be greener and less expensive than traditional methods. However, there are only a few studies of this topic which performances are satisfactory [10,11].

It is well known that the gas chromatography method is simple and preferable for quantitative analysis in cyclohexene epoxidation [12–14]. However, recently, there has been considerable discussion on the effect of temperature in injection port and column to the chromatographic selectivity values of observed products. Similar phenomena have been described for other reactions, such as the alkylation of imidazole [15]. As we noted in a previous study [16], some of new products, which could not be realized in the reaction media, can be further formed inside the injection port (at 220 °C) and the column (at 180 °C). For example, cyclohexane 1,2-diol, 2-cyclohexene-1-ol and 2-cyclohexene-1-one might be observed by gas chromatography analyses, although Raman result suggested that 1,2-epoxycyclohexane was the only product obtained in the reaction. It is important to mention that among many powerful techniques, which might be used to provide unique fingerprints for molecular analysis and monitoring of chemical reactions, Raman spectroscopy is particularly suitable to study *in situ* catalytic reaction [17–22]. Considering them together in this study, gas chromatography is used to screen the catalytic activity by determining cyclohexene conversion values while Raman technique is used to identify the reactants and selective products of epoxidation in real-time. Herein, the photo-epoxidation of cyclohexene in the presence of *t*-BuOOH was investigated for the first time over a series of V-Ti/MCM-41 photocatalysts. Additionally, the photocatalytic and thermal catalytic cyclohexene

epoxidation behaviors of these catalysts were further investigated using real-time Raman spectroscopy. Most importantly, a possible mechanism for cyclohexene photo-epoxidation was also proposed based on the results of Raman technique.

2. Results and Discussion

2.1. Catalysts Characterization

Table 1 shows the nomenclature, wt.% loading and V:Ti atomic weight ratios of series V-Ti/MCM-41 catalysts. The V:Ti atomic weight ratios measured by ICP-AES analysis are corresponded to the nominal ones. As shown in Table 2, similar results from the surface area and average pore diameter has been observed. The surface areas were in the range of 815–891 m^2/g while BJH pore diameters were within 2.9–3.0 nm. These data indicate that the structure of a series MCM-41 supported in this study is very uniform.

Table 1. Nomenclature, wt.% loading and atomic weight ratios of series catalysts.

Entry	Nomenclatures	V:Ti:Si atomic weight ratio [a] (nominal)			V loading [b] (wt.%)	Ti loading [b] (wt.%)	V:Ti:Si atomic weight ratio [c] (ICP-AES)		
		V	Ti	Si			V	Ti	Si
1	V_2Ti_0/MCM-41	2	0	100	0.36	0	1.7	0	100
2	V_1Ti_1/MCM-41	1	1	100	0.18	0.29	0.9	1.3	100
3	$V_{0.25}Ti_2$/MCM-41	0.25	2	100	0.04	0.53	0.22	2.3	100
4	$V_{0.05}Ti_4$/MCM-41	0.05	4	100	0.01	0.96	0.06	4.2	100
5	V_0Ti_5/MCM-41	0	5	100	0	1.12	0	4.9	100

[a] Atomic weight ratio (V:Ti:Si), based on the assumption of preparation process by hydrothermal method; [b] Loading content (wt.%) of V and Ti, based on ICP-AES; [c] Atomic weight ratio (V:Ti:Si), calculated from ICP-AES.

Table 2. Specific surface area, average pores diameter and band gap of series catalysts.

Entry	Catalysts	Specific surface area (m^2/g)	BJH average pore diameter (nm)	Band gap (eV)
1	V_2Ti_0/MCM-41	856	3.0	3.1
2	V_1Ti_1/MCM-41	815	3.0	3.4
3	$V_{0.25}Ti_2$/MCM-41	891	2.9	4.5
4	$V_{0.05}Ti_4$/MCM-41	841	2.9	4.4
5	V_0Ti_5/MCM-41	850	2.9	4.3

Figure S1 (Supporting Information) shows a single and narrow pore size distribution of V-Ti/MCM-41 with various ratios of V-/Ti-loading, as estimated following the BJH method from the desorption isotherms. The V-Ti loadings changed very low so they did not appreciably change the average pore diameter of MCM-41. The pore diameters of the synthesized V-Ti/MCM-41 catalysts were near 3 nm and were not significantly affected by the presence of vanadia and titania. The results proved that our procedure to incorporate vanadium and titanium-containing catalysts did not deteriorate the MCM-41 structure.

The XRD patterns of V-Ti/MCM-41 catalysts prepared with different V-Ti ratios are shown in Figure 1. All catalysts had very similar patterns, indicating that all V-/Ti-loading into Si–O framework of MCM-41 had no apparent structure influence on its structure. All the V-Ti/MCM-41 catalysts exhibited

a hexagonal lattice of mesoporous silica structures from a clear observation of spectra featured narrow (100) peaks. Nonetheless, the (110) and (200) peaks were not well distinguished. Additionally, there was no peak assigned to metal oxides, indicating that the metal ions were atomically dispersed on the internal and/or external surfaces of MCM-41. On the other hand, the amount of V and Ti loading was quite low (Table 1) that may also led in the absence of foreign ions peaks in XRD patterns. This observation is found to consist of Raman result of $V_{0.25}Ti_2$/MCM-41 along with that of TiO_2-anatase and V_2O_5 spectral references (Figure 2). Neither of the characteristic vibrations of titania anatase (or any other titania phase) nor those of crystalline vanadia was also apparent in the Raman spectrum of fresh $V_{0.25}Ti_2$/MCM-41.

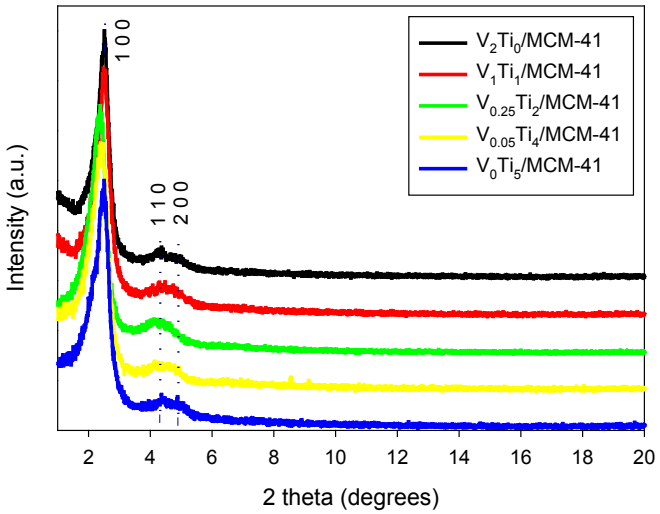

Figure 1. XRD patterns of V-Ti/MCM-41 catalysts.

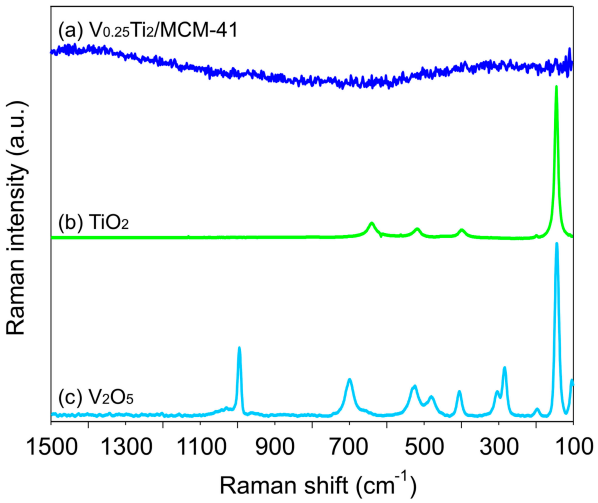

Figure 2. The 514 nm Raman spectra of (**a**) $V_{0.25}Ti_2$/MCM-41, (**b**) TiO_2 anatase and (**c**) V_2O_5 catalysts under ambient conditions.

The UV-vis spectra of catalysts with different Ti-/V-loading ratios in MCM-41 are displayed in Figure 3. The red-shift clearly increased with the growth amount of Ti-/V-loading. The spectra of Ti-loading exhibited a strong absorption band centered at about 220 nm, which was consistent with tetrahedral titania species on silica-based substrates [23]. Moreover, the presence of the peaks at 230 and 270 nm may attribute to the isolated Ti atoms in octa-coordinated Ti species and polymerized

hexa-coordinated Ti species, respectively [24,25]. On the other hand, the absorption at 220 nm shifted towards 245 nm while a second component became increasingly apparent at 340 nm when V-loading was incremented. The absorption band near 340 nm was presented due to the charge transfer bands of highly dispersed tetra-coordinated V-oxide species present to the V^{5+} state [26]. It is noted that the V^{5+} species absorbed not only at 340 nm, but also at 260 nm [27,28]. In addition, the region band of 320–350 and 400 nm might be associated to polymeric V^{5+} species and octa-coordinated vanadium, respectively [27,29]. For further investigation, the band gap of series catalysts with different amounts of Ti and V loading in MCM-41 were calculated based upon the UV-vis results and listed in the Table 2.

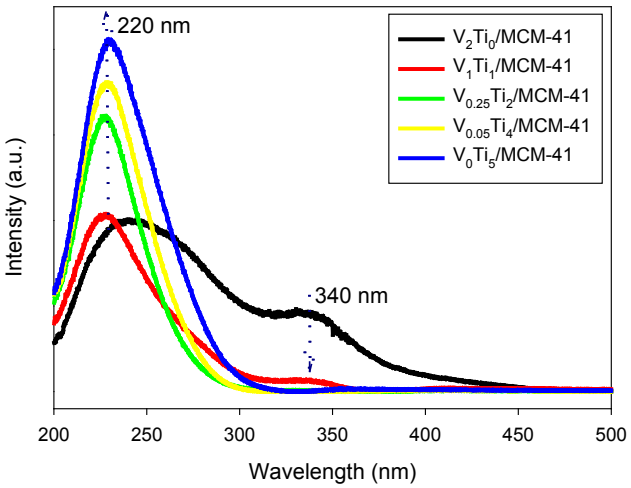

Figure 3. UV-vis spectra of the series V-Ti/MCM-41 catalysts.

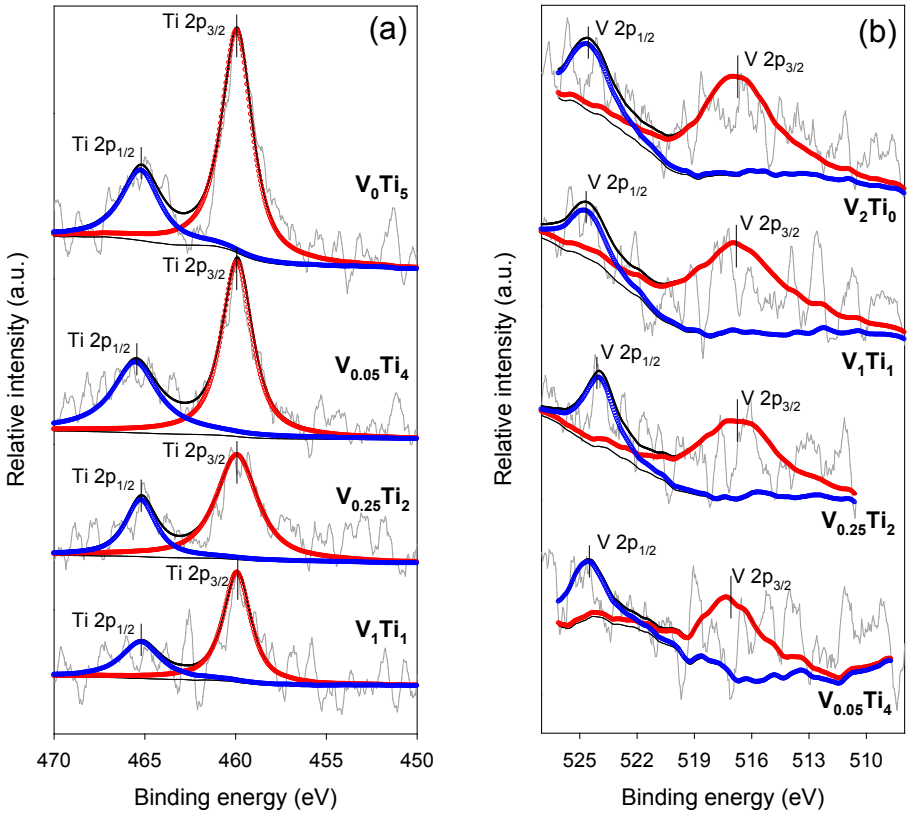

Figure 4. The XPS spectra of the series V-Ti/MCM-41 catalysts: (**a**) Ti 2p and (**b**) V 2p.

X-ray photoelectron spectroscopy (XPS) has been used to determine the electronic properties of the component existed on the surface. The XPS spectra are obtained and shown in Figure 4. For various Ti-oxide and V-oxide contents, the binding energies at 459.9 and 516.7 eV have been observed from the deconvolution of spectra for the Ti $2p_{3/2}$ and V $2p_{3/2}$ band, respectively. It is noted to mention that the binding energy of Ti $2p_{3/2}$ on silica MCM-41 was higher than that of pure TiO_2 (458.2–459.0 eV) [30]. It is possible that the high binding energy reflects the tetrahedral coordinated Ti-oxide component in the strongly interaction between titania and silica Ti–O–Si, which agrees well with the value of Ti^{4+} supported on silica (458.8–459.9 eV), reported by Castillo *et al.* [31]. Importantly, all the samples showed similar binding energy of Ti, suggesting that there is no apparent interaction between Ti and V species. On the other hand, the binding energy of V $2p_{3/2}$ was in perfect agreement with V_2O_5 (516.6–517.5 eV) [30]. Due to the little amount of V on MCM-41 (V loading in range of 0.01–0.36 wt.%), its XPS peaks could not be observed clearly. The XPS result is consistent with the observation from UV-vis.

2.2. Liquid-Phase Epoxidation of Cyclohexene

Table 3 shows the blank tests, which are examined before performing the epoxidation of cyclohexene, underline that the reaction over catalysts is essentially photocatalytic. In details, negligible epoxidation was observed either when the reactor was UV illuminated in the absence of $V_{0.25}Ti_2$/MCM-41 catalyst, or if the catalyst was run at 60 °C without UV illumination. The same phenomenon was also observed in the presence of MCM-41 under light irradiation.

Table 3. Blank test results for cyclohexene epoxidation.

Entry	Conditions			Conversion of cyclohexene (%)
	Catalyst	UV irradiation	Temp. (°C)	
1	NO	NO	80	5.5
2	NO	YES	60	3.4
3	$V_{0.25}Ti_2$/MCM-41	NO	60	0.9
4	MCM-41	YES	60	0.9

The data was collected after 6 h in reaction. Cyclohexene conversion = 100% × (moles of initial cyclohexene—Moles of final cyclohexene)/moles of initial cyclohexene.

2.2.1. Effect of V-Ti/Si Weight Ratio on the Photocatalytic Epoxidation

The effect of V-Ti/Si ratio on the photocatalytic epoxidation activity is summarized in Table 4. In the presence of single active sites, V_0Ti_5/MCM-41 achieves high conversion to 1,2-epoxycyclohexane (47%) while V_2Ti_0/MCM-41 receives only 37% of conversion. We might conclude that both V- and Ti-loading can be responsible for the cyclohexene epoxidation. The complementary behavior of V- and Ti-loading may be related to a similar role of activation. We will discuss this in greater detail later in the next section. It is noted that the weight percent of V-/Ti-loading in V_2Ti_0/MCM-41 and V_0Ti_5/MCM-41 are 0.36% and 1.12%, respectively. Therefore, V_0Ti_5/MCM-41, as expected, would be more effectively than that of V_2Ti_0/MCM-41. In the presence of dual active sites, V_1Ti_1/MCM-41 promotes the best efficiency (44%), among the candidates. Moreover, decrease the V/Ti ratio will also result on the decline the photo-reaction efficiency.

Table 4. Photocatalytic epoxidation at 60 °C for 6 h using various V-Ti weight ratios.

Entry	Catalysts	V/Ti ratio	Conversion of cyclohexene (%)
1	V_2Ti_0/MCM-41	-	37
2	V_1Ti_1/MCM-41	1	44
3	$V_{0.25}Ti_2$/MCM-41	0.125	35
4	$V_{0.05}Ti_4$/MCM-41	0.0125	38
5	V_0Ti_5/MCM-41	-	47

Cyclohexene conversion = 100% × (moles of initial cyclohexene − moles of final cyclohexene)/moles of initial cyclohexene.

2.2.2. Catalytic and Photocatalytic Activity Comparison on $V_{0.25}Ti_2$/MCM-41 Catalyst

Additional epoxidation experiments were carried out to gain better insight on the role of photo/thermal driving forces. All reactions were compared in the presence of $V_{0.25}Ti_2$/MCM-41 catalyst under different temperature with/without UV irradiation, as shown in Figure 5. In more details, reaction at 80 °C without UV irradiation delivers 10.9% of conversion. The decreasing reaction temperature from 80 °C to 60 °C in the dark results in no appreciable activity within 6 h. Conversely, reaction at 60 °C under UV irradiation achieves 23.2% while reaction at 25 °C under UV irradiation delivers only 2.1% of conversion. It is worthwhile to mention that negligible epoxidation was also observed in the presence of bare MCM-41 under light irradiation (Table 3). Taking those results into consideration, the epoxidation over $V_{0.25}Ti_2$/MCM-41 catalyst takes place as a consequence of both photo-assisted and thermal reactions.

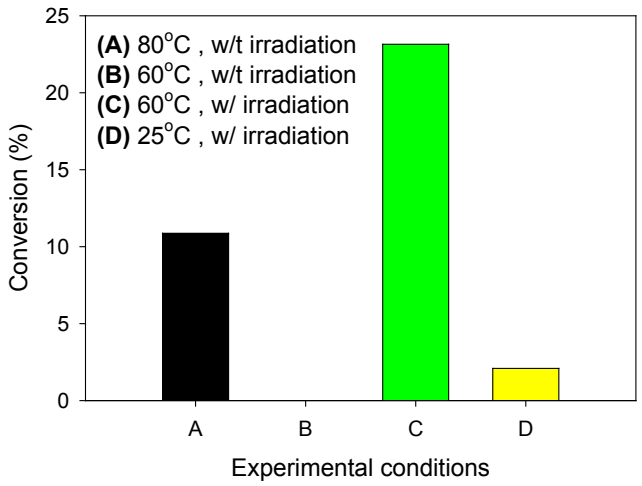

Figure 5. Catalytic and photocatalytic epoxidation of cyclohexene over $V_{0.25}Ti_2$/MCM-41 catalyst for 6 h under different conditions: (**A**) 80 °C, without irradiation; (**B**) 60 °C, without irradiation; (**C**) 60 °C, with irradiation; and (**D**) 25 °C, with irradiation.

2.3. Real-time Raman Monitoring of Cyclohexene Epoxidation

Figure 6 shows real-time Raman monitoring during epoxidation of cyclohexene with *t*-BuOOH over $V_{0.25}Ti_2$/MCM-41 catalyst under UV-light irradiation at 60 °C. The photocatalytic reaction was monitored by Raman spectroscopy without the interference of UV light. The full range spectra of

representative Raman spectra during the reaction are illustrated in Figure 6a. The characteristic Raman bands of reactant (cyclohexene), oxidant (*t*-BuOOH) and product (1,2-epoxycyclohexane) correspond to those of the reference compounds (Figure S2–S4, Supporting Information). For more details, Figure 6b shows representative Raman bands of both reactants and final product. The Raman peak of 1,2-epoxycyclohexane at 784 cm^{-1} grows while those peaks belonging to cyclohexene and *t*-BuOOH decrease simultaneously. The most interesting result has been observed that no other Raman peaks are apparent during this reaction; thus, the Raman spectra confirms that 1,2-epoxycyclohexane is obtained as the only reaction product (100% selectivity) by photocatalytic epoxidation. Additionally, Raman spectra delivers further insight into the photo-reaction mechanism. The inset of Figure 6b shows an isosbestic point near 800 cm^{-1}, between the decreasing Raman band of cyclohexene at 824 cm^{-1} and the increasing band of the epoxide at 784 cm^{-1}; these indicate that there is no stable intermediate species formed during the photo-epoxidation of cyclohexene into 1,2-epoxycyclohexane.

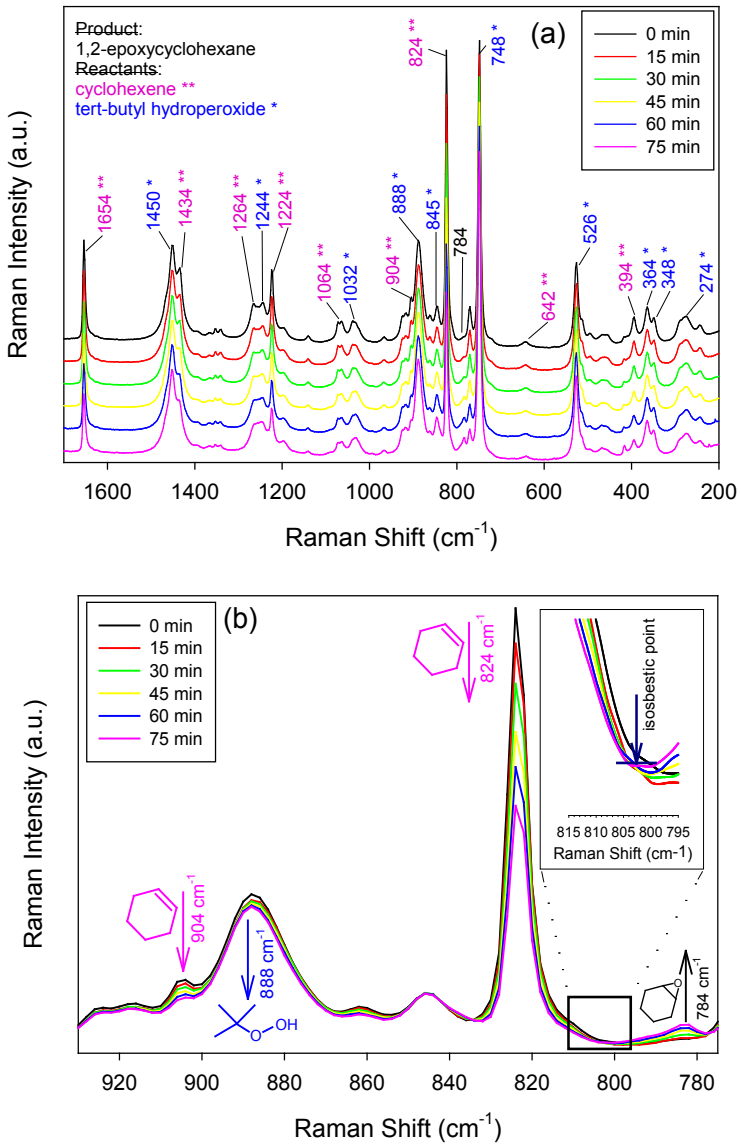

Figure 6. Representative Raman spectra during the photocatalytic cyclohexene epoxidation with *t*-BuOOH over $V_{0.25}Ti_2$/MCM-41 catalyst at 60 °C for 75 min: (**a**) full spectra; (**b**) partial spectra in range of 775–930 (cm^{-1}).

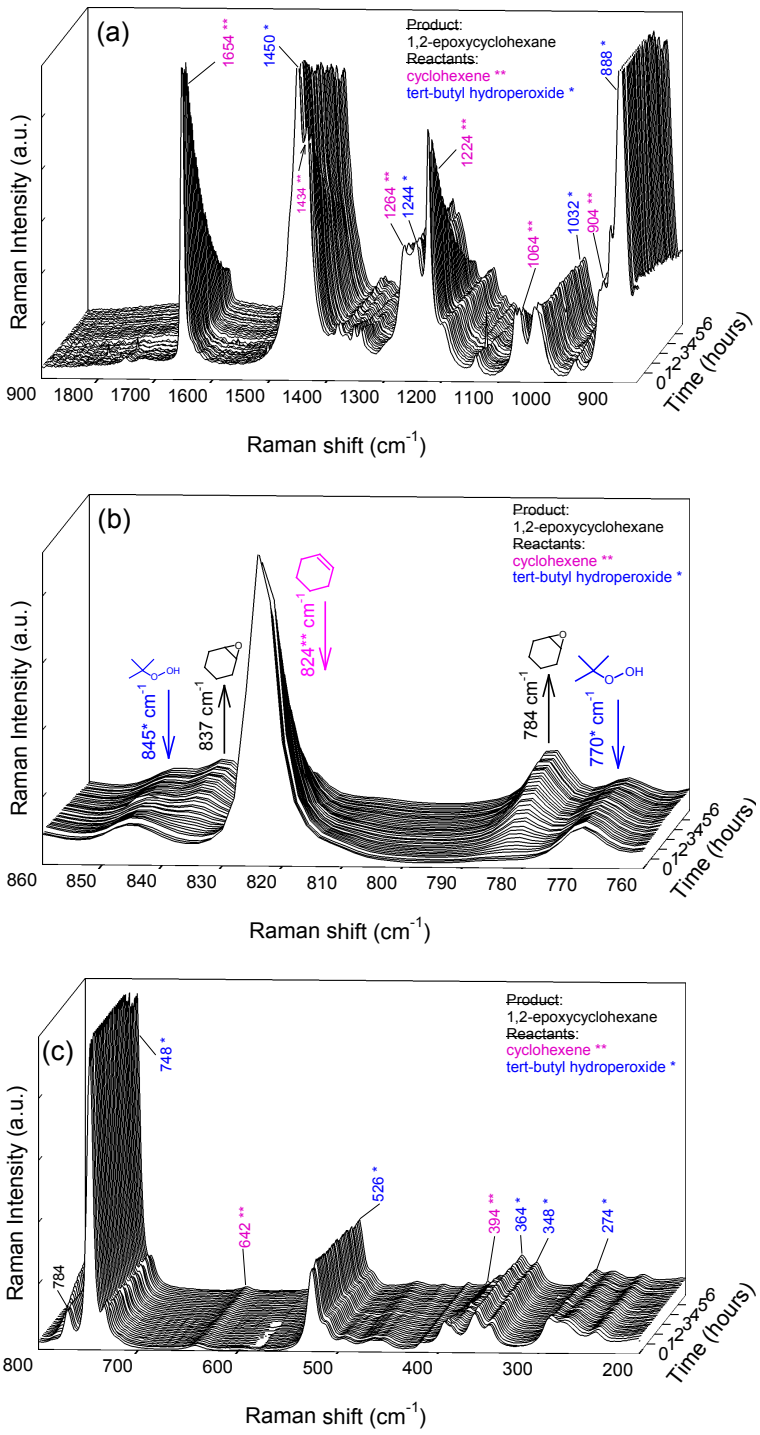

Figure 7. Representative Raman spectral range of (**a**) 1900–860 cm^{-1}; (**b**) 860–760 cm^{-1}; and (**c**) 800–200 cm^{-1} during the thermal catalytic epoxidation of cyclohexene with *t*-BuOOH over $V_{0.25}Ti_2$/MCM-41 catalyst at 80 °C for 6 h.

For comparative purposes, we performed the thermal epoxidation of cyclohexene in *t*-BuOOH on $V_{0.25}Ti_2$/MCM-41 catalyst at 80 °C without UV-light. Figure 7a–c show representative spectra range of 1900–860 cm^{-1}, 860–760 cm^{-1} and 800–200 cm^{-1}, respectively, that recorded every 10 min during reaction. It is clearly observed Raman bands of the reactant (cyclohexene) and the oxidant (*t*-BuOOH) decrease in intensity and the product (1,2-epoxycyclohexane) increases in intensity during time-on-stream. Figure 7b illustrates a zoom into the window with representative Raman bands of the participating

species, showing the consumption of cyclohexene (824 cm^{-1}); those of *t*-BuOOH (770 cm^{-1} and 845 cm^{-1}) hardly changed in intensity during reaction since it is supplied in excess. It should be noted that the 1,2-epoxycyclohexane (784 cm^{-1}) is gradually produced. In brief summary, $V_{0.25}Ti_2$/MCM-41 catalyst is not only successful in the epoxidation of cyclohexene under UV-light irradiation but it can also work in the dark at higher temperature, 80 °C. Furthermore, Real-time Raman spectra did not find any interaction between organic compounds and the active sites of the catalyst.

2.4. Proposed Photo-Mechanism for the Formation of Cyclohexene Epoxidation

Our UV-vis and XPS results indicate that V- and Ti-loading, which are separately well-dispersed in the mesoporous MCM-41, mainly exist in the tetra-coordinated (4-folds coordination). Thus, they can be easily excited under UV-light irradiation to form the corresponding charge-transfer excited states involving an electron transfer from O^{2-} species to V^{5+} and Ti^{4+} species, respectively (Equations (1) and (2)) [32–34].

$$[V^{5+}=O^{2-}] \leftrightarrows [V^{4+}-O^{-}]^* \quad (1)$$

$$[Ti^{4+}-O^{2-}] \leftrightarrows [Ti^{3+}-O^{-}]^* \quad (2)$$

It is in agreement that the high reactivity of these charge-transfer excited state is possible due to the electron-hole pair states are localized in close proximity [33]. On the other hand, Raman result suggests that cyclohexene is directly photo-epoxidized to 1,2-epoxycyclohexane in the presence of *t*-BuOOH. Taking into account these results, a possible photo-epoxidation mechanism by highly dispersed V-oxides and Ti-oxides single-site photocatalysts is proposed, as seen in Scheme 1. Firstly, either V^{5+} or Ti^{4+} species is photo-excited to $[V^{4+}-O^{-}]^*$ and $[Ti^{3+}-O^{-}]^*$, respectively. As mentioned above, both V- and Ti-loading can be responsible for the cyclohexene epoxidation. In addition, the complementary behavior of V- and Ti-loading may be related to a similar role of activation. Therefore, these photo-excited state species, within their lifetimes, are able to react with *t*-BuOOH to form (tBuO$^-$) radical, which is responsible for the formation of 1,2-epoxycyclohexane.

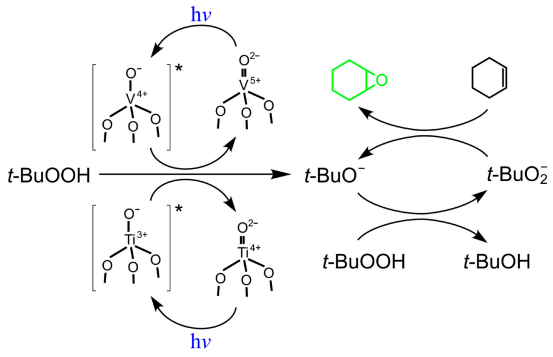

Scheme 1. Proposed photo-mechanism via vanadium and titanium active species during photocatalytic epoxidation of cyclohexene with *tert*-butyl hydroperoxide (*t*-BuOOH).

When both of V-oxides and Ti-oxides present, it might interact together to further enhance efficiency. In a previous study, Davydov *et al.* proposed that the charge separation occurred with a hole and an electron in Ti-O species [35]. In particular, the Cr^{5+} species of $[Cr^{5+}-O^{-}]^*$ can donate an electron into

the surrounding Ti–O moieties while O^- could scavenge an electron from the surrounding Ti–O moieties. It is important to note that vanadium ions would similarly undergo an equivalent charge transition to $[V^{4+}–O^-]^*$ excited states because V^{5+} and Cr^{6+} ions have the same electronic structure [34]. Therefore, the charges, which might happen at or near the photocatalyst's surface, can induce the photo-epoxidation by either direct excitation via Ti–O moieties or indirect excitation via charge transition from $[V^{4+}–O^-]^*$ states. As a result, the existence of both V- and Ti-loading will further enhance the efficiency of reaction.

3. Experimental Section

3.1. Preparation of Catalysts

The mesoporous V-Ti/MCM-41 catalysts were prepared by a hydrothermal method, which was based on a procedure described by Hung *et al.* [36], using the following general gel composition (molar ratios) 1 SiO_2: 0.2 CTAB: 0.89 H_2SO_4: 120 H_2O. In our research, we named each catalyst with different metal loading weight ratios (V-Ti-Si), such as (2-0-100), (1-1-100), (0.25-2-100), (0.05-4-100), (0-5-100). The whole synthesis procedure is shown in Scheme 2.

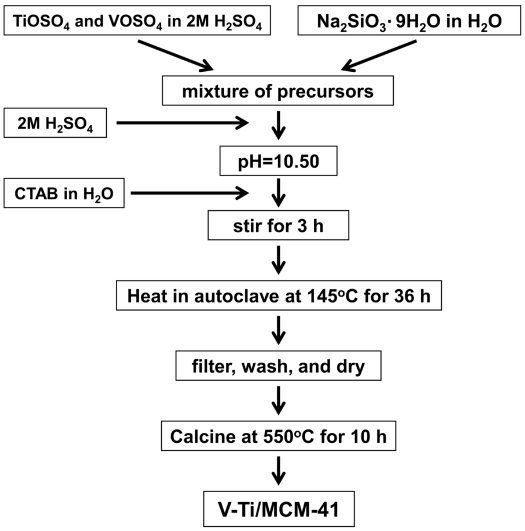

Scheme 2. Flow chart for synthesis procedure of V-Ti/MCM-41 photocatalysts.

In a typical synthesis procedure, 21.2 g of sodium metasilicate monohydrate (J.T.Baker, Avantor Performance Materials, Center Valley, PA, USA) dissolved in 100 mL of distilled water is combined with the appropriate amount of titanium oxysulfate hydrate (Sigma-Aldrich, St. Louis, MO, USA) and/or vanadyl sulfate hydrate (Acros, Geel, Belgium) metal precursors (dissolved in 20 mL of 2 M H_2SO_4 (95%–97%, Sigma-Aldrich)), respectively. The resulting mixture is stirred vigorously for 30 min. Then, 2 M H_2SO_4 is added to the above mixture to adjust the pH to 10.5 while constantly stirring to form a uniform gel. After stirring, the solution containing 7.28 g cetyltrimethylammonium bromide (CTAB, 98%, Alfa Aesar, Haverhill, MA, USA) is dissolved in 25 mL of distilled water and is added slowly into the above mixture and the combined mixture is stirred for three additional hours. The CTAB surfactant was used as the structure-directing template. The resulting gel mixture is transferred into a Teflon coated autoclave and kept in an oven at 145 °C for 36 h. After cooling to room temperature, the resulting solid

is recovered, washed and dried in an oven at 80 °C for 8 h at least. Finally, the organic template is removed after calcination at 550 °C for 10 h.

3.2. Characterization of Catalysts

Powder X-ray diffraction (XRD) data was obtained on a Panalytical X'Pert Pro diffractometer (Almelo, Netherlands) to verify the crystalline structure. The diffraction patterns were checked and assigned to known crystalline phases. The light absorption of photocatalysts was fully characterized by UV-vis spectroscopy (UV-vis, Varian Cary 100, Agilent Technologies, Santa Clara, CA, USA). The Inductively Coupled Plasma—Atomic Emission Spectra (ICP-AES) Analysis was carried out by PerkinElmer Optima 2000 (PerkinElmer, Waltham, MA, USA) to determine the chemical composition of the V, Ti and Si elements in V-Ti/MCM-41 catalysts. X-ray photoelectron spectroscopy (XPS) was conducted on a Thermo Theta Probe instrument (Thermo Fisher Scientific Inc., East Grinstead, UK) to determine the electronic properties of the component existed on the surface. Additionally, nitrogen adsorption and desorption isotherms, surface area, and mesopore size distribution were measured using a Micromeritics ASAP2000 (Micromeritics, Norcross, GA, USA). Specific surface areas and pore size distributions were calculated using the Brunnauer-Emmett-Teller (BET) and Barrett-Joyner-Halenda (BJH) methods, respectively. Furthermore, Raman spectra for the characterization of the solid catalysts were obtained with a single monochromator Renishaw Raman System 1000 (Renishaw, Gloucestershire, UK) equipped with a thermoelectrically cooled CCD detector (−73 °C) and holographic Edge filter. The samples were excited with the 514 nm Ar line. The spectral resolution was 3 cm^{-1}, and the spectrum acquisition was 300 s for each sample.

3.3. Liquid-Phase Photocatalytic Epoxidation of Cyclohexene

The experiments of liquid-phase photocatalytic epoxidation of cyclohexene were performed in a three-neck round-bottom flask reactor equipped with a reflux condenser in a temperature-controlled oil bath as shown in Scheme 3. Initially, 50 mmol of *tert*-butyl hydroperoxide (*t*-BuOOH, Aldrich, 70% in water) and 5 mol% of catalysts were added to the reactor. After that, the reaction mixture was magnetically stirred and heated until the desired reaction temperature (25 °C, 60 °C and 80 °C, respectively). The reaction was started by adding 25 mmol of cyclohexene (99%, Alfa Aesar, Haverhill, MA, USA) to the mixture. The UV-light was irradiated from EXFO S1500 (EXFO Inc., Quebec, Canada) equipped with 200W Mercury-Arc lamp (0.5 mW/cm^2, filter: 320–500 nm) and guided by an optical fiber that can insert into the three-necked reactor. The light intensity was detected at the output of optical fiber by GOLDILUX Radiometer/Photometer (UV-A Probe/UV-C Probe). Reproducibility tests were run on several catalysts to confirm the accuracy of experiments that we assured the error on photocatalytic reactions were within 10%. Since the effect of Raman is a millionth to ten millionths weaker than Rayleigh scattering, any residual light at longer wavelengths from the UV light source had to be filtered off. To do so, a filter rejecting any radiation with wavelength longer than 750 nm (Thorlabs, FM201) was located between UV-light source and the sample. Its transmittance was 100% below 750 nm.

The liquid-phase cyclohexene epoxidation was continuously monitored by Raman spectroscopy with an in Photonics immersion probe fitted to a Perkin-Elmer Raman Station 400F system (Perkin-Elmer Inc., Shelton, CT, USA), equipped with a thermoelectrically cooled CCD detector (−73 °C) and Edge

filter. The NIR filter located at the UV-light source prevented any interference from residual longer wavelengths. All the spectra were acquired every 10 min upon excitation with a near-infrared 785 nm excitation line and consisted of 6 accumulations of 10 s. The quantitative analysis of Raman spectra based on the multivariate methods analysis. The collected spectra (which include reactants and product) were analyzed by the evaluation Spectrum QUANT + V4.51 software (PerkinElmer). A partial least squares (PLS) regression was done and the calibration data, which use different calibration compositions (20 standards) of cyclohexene and 1,2-epoxycyclohexane , were stored with a correlation coefficient R^2 more than 99% and an average error of analysis less than 2%.

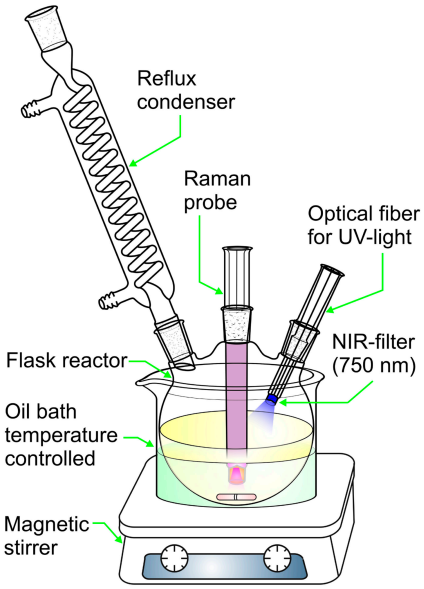

Scheme 3. Reaction system for the liquid-phase epoxidation: (1) reflux condenser; (2) three-neck flask reactor; (3) temperature-controlled oil bath; (4) Raman probe; (5) optical fiber for UV-light irradiation; (6) NIR-filter (750 nm) integrated with optical fiber; and (7) magnetic stirrer.

Additionally, reaction samples before and after 6 h in reaction were also analyzed by gas chromatography in an YL6100 GC equipped with a Porapak-N column and a flame ionization detector (FID). The cyclohexene conversion was defined in Equation (3).

$$\text{Cyclohexene conversion} = 100\% \times (\text{moles of initial cyclohexene} - \text{moles of final cyclohexene})/\text{moles of initial cyclohexene} \quad (3)$$

4. Conclusions

A series of V- and/or Ti-loading MCM-41 catalysts are successfully synthesized with a hydrothermal method. At low metal loading, of both vanadium and titanium ions, which mainly exists as tetrahedral coordination, are well dispersed to the Si–O framework. Both V- and Ti-loading can be responsible for the cyclohexene epoxidation. Moreover, the complementary behavior of V- and Ti-loading may be related to a similar role of activation. On the other hand, real-time Raman monitoring during thermo-photocatalytic cyclohexene epoxidation is for the first time successfully conducted without interference from UV-light irradiation. The results indicate that cyclohexene is directly photo-epoxidized to 1,2-epoxycyclohexane

in the presence of *t*-BuOOH, thus, it runs directly with no stable intermediate. A possible mechanism of cyclohexene photo-epoxidation was proposed based on the Raman result.

Acknowledgments

We gratefully acknowledge the National Science Council of Taiwan for financial support of this research under contract number NSC 99-2923-E-002-002-MY2 (Taiwan), CTQ2011-13343-E (Spain) and bilateral NSC-CSIC project 2009TW0021.

Author Contributions

H.-Y. Chan, J.C.S. Wu, M.A. Bañares and H. Bai conceived and designed the research concept; V. Calvino-Casilda and H.-Y. Chan prepared the setup and performed the experiments; H.-Y. Chan, V.-H. Nguyen and V. Calvino-Casilda analyzed the data; V. Calvino-Casilda, M.A. Bañares, V.-H. Nguyen and J.C.S. Wu prepared the manuscript; and V.-H. Nguyen and J.C.S. Wu finished the manuscript.

Conflicts of Interest

The authors declare no conflict of interest.

References

1. Oyama, S.T. Rates, Kinetics, and Mechanisms of Epoxidation: Homogeneous, Heterogeneous, and Biological Routes. In *Mechanisms in Homogeneous and Heterogeneous Epoxidation Catalysis*; Oyama, S.T., Ed.; Elsevier: Amsterdam, The Netherlands, 2008; pp. 3–99.
2. Nguyen, V.-H.; Chan, H.-Y.; Wu, J.C.S.; Bai, H. Direct gas-phase photocatalytic epoxidation of propylene with molecular oxygen by photocatalysts. *Chem. Eng. J.* **2012**, *179*, 285–294.
3. Nguyen, V.-H.; Chan, H.-Y.; Wu, J. Synthesis, characterization and photo-epoxidation performance of Au-loaded photocatalysts. *J. Chem. Sci.* **2013**, *125*, 859–867.
4. Nguyen, V.-H.; Wu, J.C.S.; Bai, H. Temperature effect on the photo-epoxidation of propylene over V-Ti/MCM-41 photocatalyst. *Catal. Commun.* **2013**, *33*, 57–60.
5. Nguyen, V.-H.; Lin, S.D.; Wu, J.C.-S.; Bai, H. Artificial sunlight and ultraviolet light induced photo-epoxidation of propylene over V-Ti/MCM-41 photocatalyst. *Beilstein J. Nanotechnol.* **2014**, *5*, 566–576.
6. Nguyen, V.-H.; Lin, S.D.; Wu, J.C.S.; Bai, H. Influence of co-feeds additive on the photo-epoxidation of propylene over V-Ti/MCM-41 photocatalyst. *Catal. Today* **2015**, *245*, 186–191.
7. Kim, I.; Kim, S.M.; Ha, C.-S.; Park, D.-W. Synthesis and cyclohexene oxide/carbon dioxide copolymerizations of zinc acetate complexes bearing bidentate pyridine-alkoxide ligands. *Macromol. Rapid Commun.* **2004**, *25*, 888–893.
8. Anaya de Parrodi, C.; Juaristi, E. Chiral 1,2-amino alcohols and 1,2-diamines derived from cyclohexene oxide: recent applications in asymmetric synthesis. *Synlett* **2006**, *2006*, 2699–2715.

9. Gago, S.; Rodríguez-Borges, J.E.; Teixeira, C.; Santos, A.M.; Zhao, J.; Pillinger, M.; Nunes, C.D.; Petrovski, Ž.; Santos, T.M.; Kühn, F.E.; *et al.* Synthesis, characterization and catalytic studies of bis(chloro)dioxomolybdenum(VI)-chiral diimine complexes. *J. Mol. Catal. A* **2005**, *236*, 1–6.
10. Li, G.; Xu, M.; Larsen, S.C.; Grassian, V.H. Photooxidation of cyclohexane and cyclohexene in BaY. *J. Mol. Catal. A* **2003**, *194*, 169–180.
11. Larsen, R.G.; Saladino, A.C.; Hunt, T.A.; Mann, J.E.; Xu, M.; Grassian, V.H.; Larsen, S.C. A Kinetic Study of the Thermal and Photochemical Partial Oxidation of Cyclohexane with Molecular Oxygen in Zeolite Y. *J. Catal.* **2001**, *204*, 440–449.
12. Fraile, J.M.; García, J.I.; Mayoral, J.A.; Vispe, E. Optimization of cyclohexene epoxidation with dilute hydrogen peroxide and silica-supported titanium catalysts. *Appl. Catal. A* **2003**, *245*, 363–376.
13. Anand, C.; Srinivasu, P.; Mane, G.P.; Talapaneni, S.N.; Benzigar, M.R.; Vishnu Priya, S.; Al-deyab, S.S.; Sugi, Y.; Vinu, A. Direct synthesis and characterization of highly ordered cobalt substituted KIT-5 with 3D nanocages for cyclohexene epoxidation. *Micropor. Mesopor. Mat.* **2013**, *167*, 146–154.
14. Jin, F.; Chen, S.-Y.; Jang, L.-Y.; Lee, J.-F.; Cheng, S. New Ti-incorporated MCM-36 as an efficient epoxidation catalyst prepared by pillaring MCM-22 layers with titanosilicate. *J. Catal.* **2014**, *319*, 247–257.
15. Calvino Casilda, V.; Pérez-Mayoral, E.; Bañares, M.A.; Lozano Diz, E. Real-time Raman monitoring of dry media heterogeneous alkylation of imidazole with acidic and basic catalysts. *Chem. Eng. J.* **2010**, *161*, 371–376.
16. Mikolajska, E.; Calvino-Casilda, V.; Bañares, M.A. Real-time Raman monitoring of liquid-phase cyclohexene epoxidation over alumina-supported vanadium and phosphorous catalysts. *Appl. Catal. A* **2012**, *421–422*, 164–171.
17. Schmink, J.R.; Holcomb, J.L.; Leadbeater, N.E. Use of raman spectroscopy as an *in situ* tool to obtain kinetic data for organic transformations. *Chem. Eur. J.* **2008**, *14*, 9943–9950.
18. Moreno, T.; Morán López, M.A.; Huerta Illera, I.; Piqueras, C.M.; Sanz Arranz, A.; García Serna, J.; Cocero, M.J. Quantitative Raman determination of hydrogen peroxide using the solvent as internal standard: Online application in the direct synthesis of hydrogen peroxide. *Chem. Eng. J.* **2011**, *166*, 1061–1065.
19. Mozharov, S.; Nordon, A.; Littlejohn, D.; Wiles, C.; Watts, P.; Dallin, P.; Girkin, J.M. Improved Method for Kinetic Studies in Microreactors Using Flow Manipulation and Noninvasive Raman Spectrometry. *J. Am. Chem. Soc.* **2011**, *133*, 3601–3608.
20. Calvino-Casilda, V.; Banares, M.A. Recent advances in imaging and monitoring of heterogeneous catalysts with Raman spectroscopy. In *Catalysis*; The Royal Society of Chemistry: Cambridge, UK, 2012; Volume 24, pp. 1–47.
21. Bañares, M.A. Operando methodology: Combination of *in situ* spectroscopy and simultaneous activity measurements under catalytic reaction conditions. *Catal. Today* **2005**, *100*, 71–77.
22. Salkic, S.; Eckler, L.H.; Nee, M.J. Noninvasive monitoring of photocatalytic degradation of X-ray contrast media using Raman spectrometry. *J. Raman Spec.* **2013**, *44*, 1746–1752.
23. Gao, X.; Wachs, I.E. Titania–silica as catalysts: molecular structural characteristics and physico-chemical properties. *Catal. Today* **1999**, *51*, 233–254.

24. Choi, J.S.; Kim, D.J.; Chang, S.H.; Ahn, W.S. Catalytic applications of MCM-41 with different pore sizes in selected liquid phase reactions. *Appl. Catal. A* **2003**, *254*, 225–237.
25. Geobaldo, F.; Bordiga, S.; Zecchina, A.; Giamello, E.; Leofanti, G.; Petrini, G. DRS UV-Vis and EPR spectroscopy of hydroperoxo and superoxo complexes in titanium silicalite. *Catal. Lett.* **1992**, *16*, 109–115.
26. Laha, S.C.; Kumar, R. Promoter-induced synthesis of MCM-41 type mesoporous materials including Ti- and V-MCM-41 and their catalytic properties in oxidation reactions. *Micropor. Mesopor. Mat.* **2002**, *53*, 163–177.
27. Arnold, A.B.J.; Niederer, J.P.M.; Nießen, T.E.W.; Hölderich, W.F. The influence of synthesis parameters on the vanadium content and pore size of [V]-MCM-41 materials. *Micropor. Mesopor. Mat.* **1999**, *28*, 353–360.
28. Lewandowska, A.E.; Banares, M.A.; Tielens, F.; Che, M.; Dzwigaj, S. Different Kinds of Tetrahedral V Species in Vanadium-Containing Zeolites Evidenced by Diffuse Reflectance UV-vis, Raman, and Periodic Density Functional Theory. *J. Phys. Chem. C* **2010**, *114*, 19771–19776.
29. Peña, M.L.; Dejoz, A.; Fornés, V.; Rey, F.; Vázquez, M.I.; López Nieto, J.M. V-containing MCM-41 and MCM-48 catalysts for the selective oxidation of propane in gas phase. *Appl. Catal. A* **2001**, *209*, 155–164.
30. Wagner, C.D.; Muilenberg, G.E. *Handbook of X-ray Photoelectron Spectroscopy: A Reference Book of Standard Data for Use in X-ray Photoelectron Spectroscopy*; Perkin-Elmer Corp., Physical Electronics Division: Eden Prairie, MN, USA, 1979; pp. 68–71.
31. Castillo, R.; Koch, B.; Ruiz, P.; Delmon, B. Influence of the Amount of Titania on the Texture and Structure of Titania Supported on Silica. *J. Catal.* **1996**, *161*, 524–529.
32. Matsuoka, M.; Anpo, M. Local structures, excited states, and photocatalytic reactivities of highly dispersed catalysts constructed within zeolites. *J. Photochem. Photobiol. C* **2003**, *3*, 225–252.
33. Anpo, M.; Kim, T.-H.; Matsuoka, M. The design of Ti-, V-, Cr-oxide single-site catalysts within zeolite frameworks and their photocatalytic reactivity for the decomposition of undesirable molecules—The role of their excited states and reaction mechanisms. *Catal. Today* **2009**, *142*, 114–124.
34. Zou, J.-J.; Liu, Y.; Pan, L.; Wang, L.; Zhang, X. Photocatalytic isomerization of norbornadiene to quadricyclane over metal (V, Fe and Cr)-incorporated Ti-MCM-41. *Appl. Catal. B* **2010**, *95*, 439–445.
35. Davydov, L.; Reddy, E.P.; France, P.; Smirniotis, P.G. Transition-Metal-Substituted Titania-Loaded MCM-41 as Photocatalysts for the Degradation of Aqueous Organics in Visible Light. *J. Catal.* **2001**, *203*, 157–167.
36. Hung, C.; Bai, H.; Karthik, M. Ordered mesoporous silica particles and Si-MCM-41 for the adsorption of acetone: A comparative study. *Sep. Purif. Technol.* **2009**, *64*, 265–272.